Scientific Reports

https://doi.org/10.1038/s41598-026-43810-3

Article in Press

Biomechanical investigation of spinal cord stress changes following ACAF for different subtypes of cervical OPLL

Received: 12 November 2025

Accepted: 6 March 2026

Published online: 17 March 2026

Cite this article as: Zhang X., Gu W., Cao D. *et al.* Biomechanical investigation of spinal cord stress changes following ACAF for different subtypes of cervical OPLL. *Sci Rep* (2026). https://doi.org/10.1038/s41598-026-43810-3

Xiao Zhang, Wenbo Gu, Donghui Cao, Xusheng Li, Hongyang Zhao, Yu Yang, Xi Zhu & Haifeng Yuan

Biomechanical Investigation of Spinal Cord Stress Changes Following ACAF for Different Subtypes of Cervical OPLL

Xiao Zhang[1,2†], Wenbo Gu[1†], Donghui Cao[1,2], Xusheng Li[1], Hongyang Zhao[2], Yu Yang[2], Xi Zhu[1], Haifeng Yuan[1,2,*]

1.General Hospital of Ningxia Medical University, Ningxia, 750004, China.

2.Ningxia Medical University, Ningxia, 750004, China.

†The two authors contributed equally to this work.

*Correspondence: yuan18709571510@163.com

Abstract

Objective: To investigate the effect of the Anterior Controllable Antedisplacement and Fusion (ACAF) procedure on stress within the spinal cord, nerve roots, and dura mater for different subtypes of cervical ossification of the posterior longitudinal ligament (C-OPLL) during progressive anterior decompression.

Methods: C2-C7 cervical spine and spinal cord models were constructed based on CT images. Three C-OPLL subtypes (central-plateau, central-beak, and right-beak) were modeled and subjected to simulated ACAF treatment. By simulating the anterior displacement of the vertebral ossification complex, we analyzed the static stress changes in gray matter, white matter, nerve roots and dura mater for different C-OPLL subtypes.

Results: During decompression, among the three C-OPLL subtypes, ACAF achieved the most significant spinal cord decompression in the central-plateau type, especially when the encroachment ratio was reduced from 60% to 30%. ACAF produced the greatest reduction in nerve-root and dural stress in the right-beak type of C-OPLL, especially when the encroachment ratio decreased from 60% to 40%. The decompression efficiency for the nerve roots in the right-beak type and for the dura mater in the central-plateau type plateaued when the encroachment ratio was reduced from 60% to 50% and from 40% to 30%, respectively. In the right-beak type of C-OPLL, asymmetric compression generated higher stresses on the ipsilateral side of the spinal cord complex. After continued gradual decompression, the stress values of the spinal complex gradually decreased in all three groups.

Conclusion: Our model demonstrates that all three OPLL subtypes achieve effective decompression, although the degree of stress relief varies across anatomical sites (e.g., spinal cord versus nerve

roots) in a subtype-specific manner. The model data suggest that as the residual encroachment ratio decreases to approximately 30%, the marginal benefit of further decompression in terms of stress reduction plateaus. It is important to emphasize that this value is solely a biomechanical observation derived from our model, and clinically acceptable thresholds must be determined by integrating the patient's neurological status and surgical risks.

Keywords: anterior controllable antedisplacement fusion (ACAF), ossification of the posterior longitudinal ligament (C-OPLL), cervical spine, spinal cord, strain, finite element analysis, biomechanics.

1. Introduction

Cervical ossification of the posterior longitudinal ligament (C-OPLL) is a pathological condition in which ectopic ossification of the posterior longitudinal ligament gradually compresses the cervical spinal cord, leading to sensory and motor deficits in the limbs [1]. The incidence of C-OPLL is high in East Asian populations, ranging from approximately 1.0% to 4.3% [2]. Due to its insidious onset, surgical intervention is typically required upon symptom presentation. Surgical strategies for C-OPLL can be categorized into anterior and posterior surgery based on surgical access.

Anterior surgery involves direct decompression via resection of the ossified mass, primarily through anterior cervical corpectomy and fusion (ACCF) or anterior cervical discectomy and fusion (ACDF). Although anterior decompression is more physiologic, the irregular growth pattern of the ossified mass and its high degree of canal encroachment significantly increase the risk of iatrogenic spinal cord injury during procedures such as ACCF. In particular, ACCF is technically demanding and carries risks including cerebrospinal fluid leakage and graft-related complications. Among them, ACDF is only suitable for the resection of ossifications with relatively short segments located in the intervertebral space. Posterior surgery does not involve resecting and decompressing the ossified material, but an indirect decompression technique, which mainly includes open-door laminoplasty (LAM) of the posterior cervical spine. It indirectly decompresses the spinal cord by allowing posterior drift, but may be ineffective in patients with a negative K-line and is associated with complications such as insufficient drift and C5 palsy [3].

Anterior Controllable Antedisplacement and Fusion (ACAF) is a recently described technique for multilevel cervical C-OPLL. After anterior vertebral-body partial resection, the ossified complex is advanced en bloc, converting intradural compression into visible anterior displacement while avoiding adhesion-related morbidity

[4]. This technique provides controlled and effective spinal cord decompression and is particularly effective in restoring the physiological alignment of the cord [5]. Although ACAF can be complicated by residual ossification or incomplete reduction, refinements in surgical technique continue to improve outcomes [6]. Several clinical studies have already reported good results of ACAF in spinal cord decompression [4,7,8]. However, the characteristic patterns of spinal cord stress change during ACAF decompression remain unquantified. Key questions include: How does spinal cord stress evolve during decompression? Do these patterns differ among C-OPLL subtypes? And what degree of residual ossification or incomplete decompression is clinically acceptable? These questions need to be explored in further studies.

In this study, the spinal cord stress of three C-OPLL subtypes during decompression was analyzed by using finite element analysis. A finite element model was developed from computed tomography (CT) images of a healthy volunteer to investigate the changes and differences in spinal cord stress during ACAF decompression surgery for different C-OPLL subtypes.

2.Methods

This study was reviewed and approved by the Ethics Committee of the General Hospital of Ningxia Medical University (approval code: KYLL-2023-0583). All procedures conformed to the ethical principles for medical research involving human subjects as set out in the 2013 revision of the Declaration of Helsinki. Written informed consent was obtained from the participant, including permission to publish any potentially identifiable data or images.

2.1. Modeling of the cervical spine

This study, approved by the Ethics Committee, utilized CT images from a healthy subject (26 years old, 172 cm in height, 70 kg in weight) for modeling. First, the CT images were processed using Mimics 21.0 software to generate an initial 3D model. Then, smoothing and hole-filling operations were performed in Geomagic Wrap 2021 to generate a solid model. In this study, the cortical bone was modeled by offsetting the entire bony structure inward by 0.4 mm, following established methodology [9]. Subsequently, structures including the cervical discs, articular cartilage, spinal cord, dura mater, and nerve roots were reconstructed using Siemens NX 12.0 software. Finally, model material assignment, mesh delineation, boundary and load application, ligament establishment, and biomechanical analysis were performed in Abaqus 6.14, as shown in Fig. 1A.

2.2. Construction of a spinal cord model

The three-dimensional model of the spinal cord was

constructed based on cross-sectional anatomical and imaging data [10]. We imported the spinal cord planes into Siemens NX 12.0 software, and then constructed the entities of gray matter, white matter, cerebrospinal fluid, and dura mater using the "sweep" command (shown in Fig. 1B). Both white matter and gray matter were modeled as nonlinear hyperelastic materials [11]. Due to the limitations of ordinary MRI in distinguishing the pia mater and for computational efficiency, the pia mater was not included in this model. Nerve roots were modeled based on their location and angle of travel in the intervertebral foramen, and solid elements were placed at each intervertebral foramen.

2.3. Construction of the C-OPLL model

In this study, we chose to construct a model of continuous type of ossification at the posterior margin of C4-C5 vertebrae. According to imaging typing [12], the type of C-OPLL ossification in the axial position was classified as central-plateau type, central-beak type, and right-beak type (Fig. S1 and S2).The lateral type used for the study in this article was the right-beak type. The C-OPLL canal encroachment ratio was defined as the ratio of the C-OPLL thickness to the anteroposterior diameter of the cervical spinal canal [13]. Starting from a common preoperative encroachment ratio of 60%, we simulated the ACAF procedure to progressively reduce this ratio to 50%, 40%, 30%, 20%, 10%, and 0%. This allowed us to analyze the corresponding stress changes in the spinal cord, nerve roots, and dura mater. The ossification was modeled as a simple rigid body model placed within the vertebral body. To simulate C-OPLL compression, the C2 and C7 vertebral bodies, as well as the spinal cord, were fixed in place. The posterior longitudinal ligament was ossified to apply displacement in a direction perpendicular to the spine. All material properties were obtained from previous studies [14-25]. Details are shown in Table 1.

Table 1. Material properties and element types used in the current model

Material	Material type	Material parameters	References
Cortical	Elastic	E^a=1.20×10⁴ MPa v=0.29 ρ^b=1.83×10⁻⁹ tonne/mm³	[14]
Cancellous	Elastic	E= 100 MPa v=0.29 ρ=1.00×10⁻⁹ tonne/mm³	[15,16]
C-OPLL	Rigid body	ρ=1.83×10⁻⁹ tonne/mm³	[17]
Titanium plate	Elastic	E= 1.10×10⁴ MPa v=0.36	[18]
Screw	Elastic	E= 1.10×10⁴ MPa v=0.30	[18]

PEEK cage	Elastic	E= 3.60×10^{3} MPa v=0.30	[19]
Cartilage	Elastic	E= 10 MPa v=.3 ρ=1.20×10^{-9} tonne/mm^3	[20]
White matter	Hyperelastic	μ^c= 4.1 kPa α^d = 14.7 ρ= 1.05×10^{-9} tonne/mm^3	[21]
Gray matter	Hyperelastic	μ= 4.0 kPa α= 12.5 ρ= 1.05×10^{-9} tonne/mm^3	[21]
Dura mater	Elastic	E= 80 MPa v=0.49 ρ=1.17×10^{-9} tonne/mm^3	[22]
Nerve roots	Elastic	E= 1.3 MPa v=0.3 ρ=1.00×10^{-9} tonne/mm^3	[23]
CSF	Newtonian fluid	Viscosity = 1×10^{-3}Pas	[24]
DLs	Elasticplastic	Stress-strain curve (0.03mm$^{2)}$	[25]

C-OPLL,Ossification of the Posterior Longitudinal Ligament; CSF, cerebrospinal fuid; DLs, denticulate ligaments. [a], Elasticity modulus; [b], Density; [c],Shear modulus; [d],Strain hardening index.

2.4. Construction of surgical models

The overall advancement process of ossification simulated in this model represents an idealized surgical scenario, aiming to establish a benchmark state for biomechanical analysis. The C3/4, C4/5 and C5/6 discs were removed and their upper and lower endplates of the intervertebral space were leveled, followed by resection of the anterior aspect of the C4 and C5 vertebral bodies. An interbody fusion device was installed in each space and a titanium plate measuring 64 × 16 × 2 mm was placed on the anterior edge of the vertebrae. A screw measuring 4.0×16mm was installed in each vertebra. Grooving was performed 2mm inside the base of the uncovertebral joint, allowing the ossified material complex to be completely free. To simulate the effect of tightening the screws at C4 and C5 to lift the vertebral body ossification complex, the software set the vertebral body ossification to move forward gradually until the vertebral body and the titanium plate were tightly affixed to each other, thereby achieving anterior translation of the entire ossified complex [26]. (Fig. 1D, E).

2.5. Validation of model validity

First, relative displacement of the C3–C7 spinal cord was calculated by simulating 20 ° of cervical flexion and extension, respectively, and compared with published in vivo [27]. The vertical compression experiment of the spinal cord was then performed by applying a concentrated force of size 0.08 N in the mid-section of the spinal cord, which was directed perpendicular to the direction of the long axis of the spinal cord. The resulting displacement was calculated using Abaqus 2022 and compared with published data

[28]. The model's predictions of spinal cord motion showed good agreement with established in vivo patterns (Supplementary Fig. S3), supporting its validity for subsequent stress analysis.

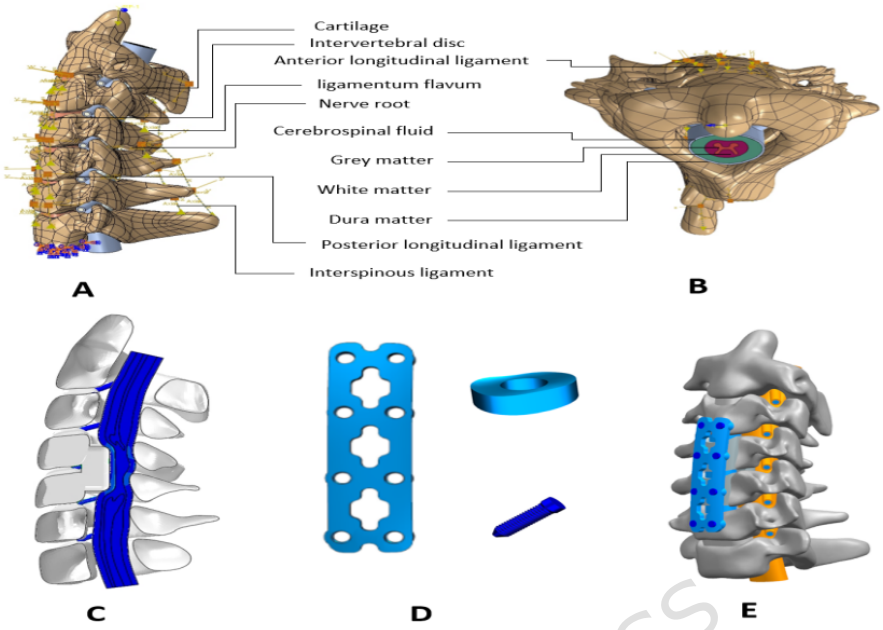

Fig. 1. The finite element model of the cervical spine and spinal cord. A: Lateral view of the cervical spine and spinal cord complex model; B: Top view of the cervical spine and spinal cord complex model; C: Schematic of the C-OPLL; D: The schematic of titanium plate, interbody fusion device, and screws; E: The schematic of complete ACAF model.

3. Results

The peak stress and strain distributions in gray matter, white matter, nerve roots, and dura mater for the three types of C-OPLL models as the encroachment ratio gradually decreased from 60% to 50%, 40%, 30%, 20%, 10%, and 0% are shown in Fig. 2-5. At the preoperative 60% encroachment ratio, the central-plateau subtype exhibited the highest peak stress in both gray and white matter among the three types. In contrast, the right-beak type of C-OPLL had the greatest peak stress on nerve roots and dura mater, and the central-beak type of C-OPLL had peak stress on gray matter, white matter, nerve roots, and dura mater in between. However, as the encroachment ratio decreased, stress on the gray matter, white matter, nerve roots, and dura mater decreased correspondingly across all C-OPLL subtypes.

3.1. Variation of peak stress in gray matter

The peak-stress pattern in the gray matter was as follows: in the central-plateau type C-OPLL, the stress values were 2.32×10^{-2}, 1.48×10^{-2}, 4.97×10^{-3}, 6.90×10^{-4}, 5.16×10^{-4}, $8.81 \times$

10^{-5}, and 7.69×10^{-10} MPa; in the central-beak type C-OPLL, the peak stresses were 1.27×10^{-2}, 1.05×10^{-2}, 2.04×10^{-3}, 5.11×10^{-4}, 4.44×10^{-4}, 5.35×10^{-5}, and 8.42×10^{-10} MPa; in the right-beak type C-OPLL, the peak stresses were 5.40×10^{-3}, 3.44×10^{-3}, 9.80×10^{-4}, 5.59×10^{-4}, 2.91×10^{-4}, 1.68×10^{-4}, and 1.25×10^{-10} MPa. When the encroachment ratio was reduced from 60% to 0%, the ACAF procedure effectively decompressed the gray matter in all three subtypes. However, the ACAF procedure provided more symmetrical and uniform decompression of the spinal cord (gray matter) in the central-plateau and central-beak types. The efficiency of gray matter decompression was most significant in the central-plateau type C-OPLL in which the encroachment ratio was reduced from 60% to 30%, followed by the central-beak type and the right-beak type. Subsequently, the reduction in gray matter stress converged across the three C-OPLL subtypes (Fig. 5A).

3.2. Variation of peak stress in white matter

The pattern of peak stress variation in the white matter is as follows: in the central-plateau type of C-OPLL, the peak stresses were 1.50×10^{-2}, 1.04×10^{-2}, 3.91×10^{-3}, 2.56×10^{-3}, 9.51×10^{-4}, 8.97×10^{-5}, and 7.44×10^{-9} MPa; in the central-beak type of C-OPLL, the peak stresses were 9.98×10^{-3}, 5.84×10^{-3}, 2.11×10^{-3}, 1.00×10^{-3}, 9.61×10^{-4}, 7.72×10^{-5}, and 7.86×10^{-9} MPa; in the right-beak type of C-OPLL, the peak stresses were 7.02×10^{-3}, 4.59×10^{-3}, 1.96×10^{-3}, 7.13×10^{-4}, 5.44×10^{-4}, 2.39×10^{-5}, and 2.19×10^{-9} MPa. The ACAF procedure showed better decompression of the white matter in these three types of C-OPLL when the encroachment ratio decreased from 60% to 0%. However, the ACAF procedure was more symmetrical and homogeneous for the decompression of the spinal cord (white matter) in the central-plateau type and the central-beak type of C-OPLL. Among them, the central-plateau type of C-OPLL had the most significant white matter decompression efficiency when the encroachment ratio was reduced from 60% to 20%, followed by the central-beak type and the right-beak type of C-OPLL. After that, the white matter stress reduction in these three types of C-OPLL converged (Fig. 5B).

3.3. Variation of peak stress in nerve roots

The variation pattern of stress in the nerve root is as follows: in the central-plateau type of C-OPLL, the peak stresses were 1.04×10^{0}, 3.95×10^{-1}, 3.31×10^{-1}, 1.86×10^{-1}, 1.34×10^{-1}, 8.88×10^{-2}, and 6.55×10^{-5} MPa; in the central-beak type of C-OPLL, the peak stresses were 4.56×10^{-1}, 3.18×10^{-1}, 2.55×10^{-1}, 1.89×10^{-1}, 1.02×10^{-1}, 6.20×10^{-2}, and 7.76×10^{-5} MPa; in the right-beak type of C-OPLL, the stress peaks were 1.22×10^{0}, 1.18×10^{0}, 3.29

× 10^{-1}, 3.06 × 10^{-1}, 1.09 × 10^{-1}, 5.54 × 10^{-2}, and 1.51 × 10^{-17} MPa. When the encroachment ratio decreased from 60% to 0%, the ACAF procedure had a good decompression effect on the nerve roots of all three types of C-OPLL, with better recovery of the nerve roots of the right-beak type of C-OPLL, and when the C-OPLL encroachment ratio decreased to 30%, the right-beak type of C-OPLL still had high stress values. However, due to the positional factors of the ossifications, the ACAF procedure was more symmetrical and homogeneous for decompression of the nerve roots in the central-plateau type and central-beak type of C-OPLL. The efficiency of nerve root decompression was most significant in central-plateau type C-OPLL when the encroachment ratio was reduced from 60% to 50%. The nerve root decompression efficiency was most significant in the right-beak type C-OPLL when the encroachment ratio was reduced from 50% to 40%. At encroachment ratios of 60%–50% and 40%–30%, the nerve root decompression efficiency of the right-beak type of C-OPLL plateaued and approximated a plateau period. After that, the stress reductions among the three C-OPLL subtypes converged (Fig. 5C).

3.4. Variation of peak stress in the dura mater

The pattern of stress change in the dura mater was as follows: in the central-plateau type of C-OPLL, the peak stresses were 5.55 × 10^{0}, 2.68 × 10^{0}, 1.63 × 10^{0}, 1.55 × 10^{0}, 8.28 × 10^{-1}, 6.31 × 10^{-1}, and 9.40 × 10^{-2} MPa; in the central-beak type of C-OPLL, the peak stresses were 3.64 × 10^{0}, 3.60 × 10^{0}, 2.19 × 10^{0}, 1.92 × 10^{0}, 1.22 × 10^{0}, 9.61 × 10^{-1}, and 1.29 × 10^{-1} MPa; in the right-beak type of C-OPLL, the stress peaks were 7.36 × 10^{0}, 4.86 × 10^{0}, 2.04 × 10^{0}, 1.99 × 10^{0}, 1.43 × 10^{0}, 1.13 × 10^{0}, and 2.37 × 10^{-14} MPa. When the encroachment ratio was reduced from 60% to 0%, the ACAF procedure achieved better decompression of the dura mater in all three types of C-OPLL. The dural decompression efficiency was most significant for the central-plateau type of C-OPLL when the encroachment ratio decreased from 60% to 50%. The dural decompression efficiency of the right-beak type C-OPLL was the most significant when the encroachment ratio was reduced from 50% to 40%. At encroachment ratios of 60 %–50 % and 40 %–30 %, the dural decompression efficiency of the central-beak type C-OPLL plateaued and approximated a plateau period. After that, the stress reduction of these three types of C-OPLL converged (Fig. 5D).

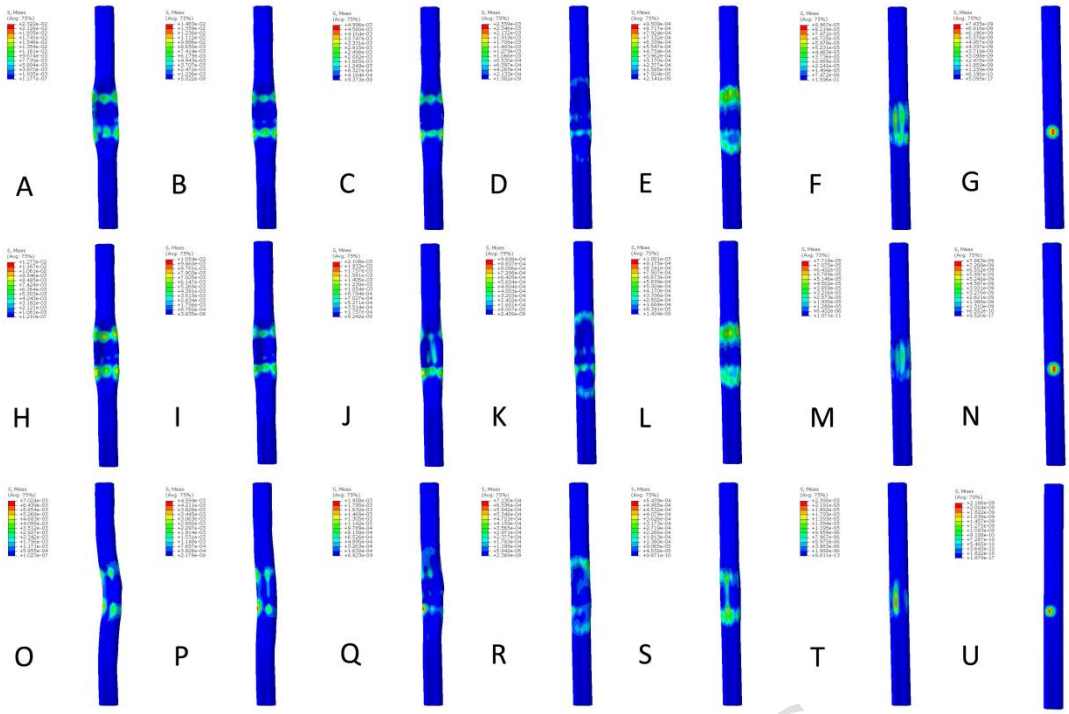

Fig. 2. Stress distribution in the anterior part of the spinal cord in three sets of C-OPLL models. A-G: central-plateau type of C-OPLL; H-N: central-beak type of C-OPLL; O-U: right-beak type of C-OPLL.

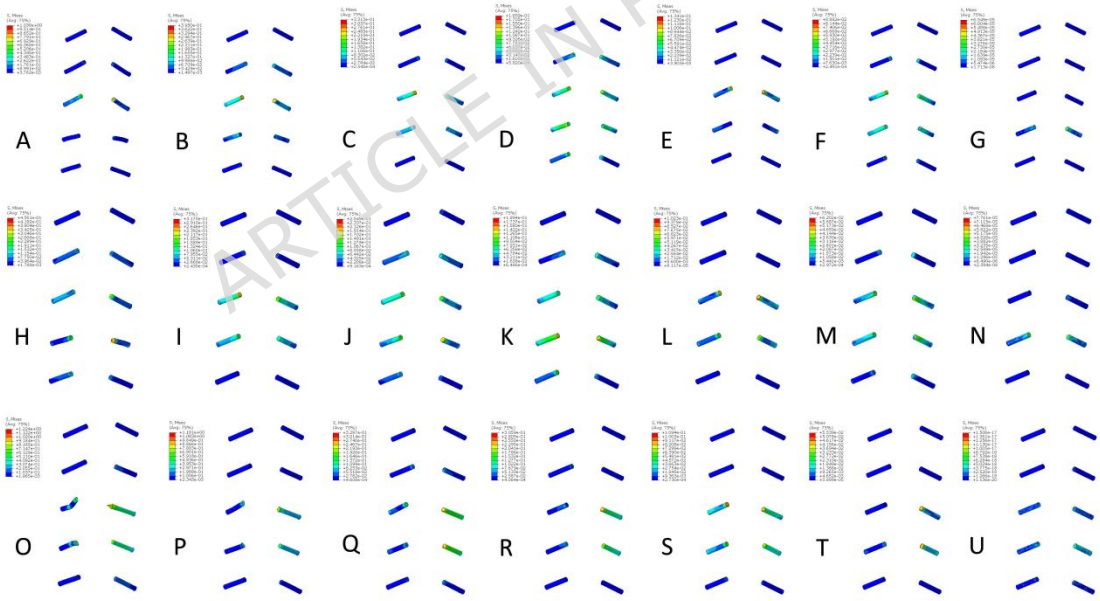

Fig. 3. Stress distribution of C3-7 nerve roots in three sets of C-OPLL models. A-G: central-plateau type of C-OPLL; H-N: central-beak type of C-OPLL; O-U: right-beak type of C-OPLL.

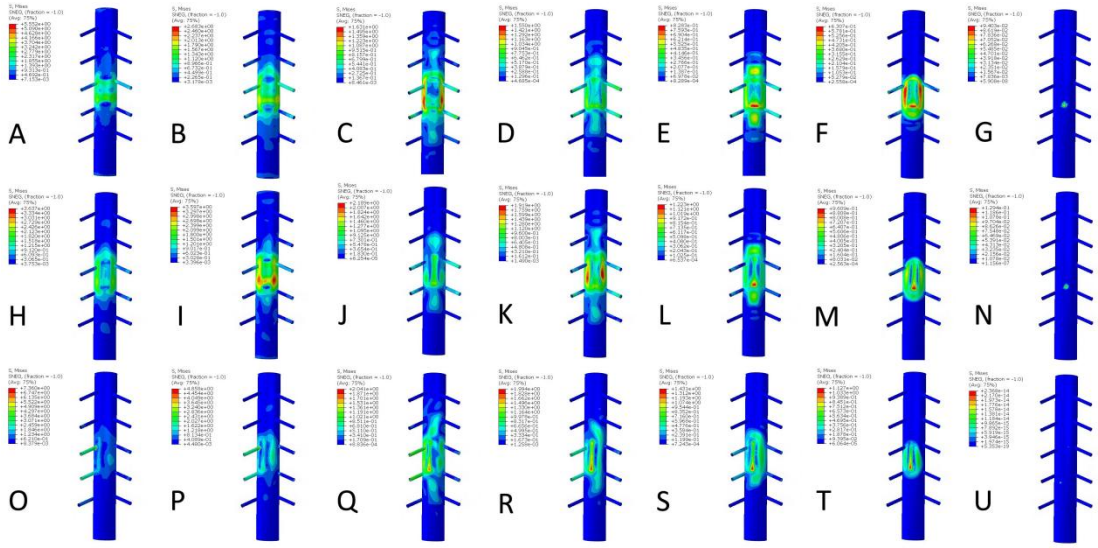

Fig. 4. Dural stress distribution in three sets of C-OPLL models. A-G: central-plateau type of C-OPLL; H-N: central-beak type of C-OPLL; O-U: right-beak type of C-OPLL.

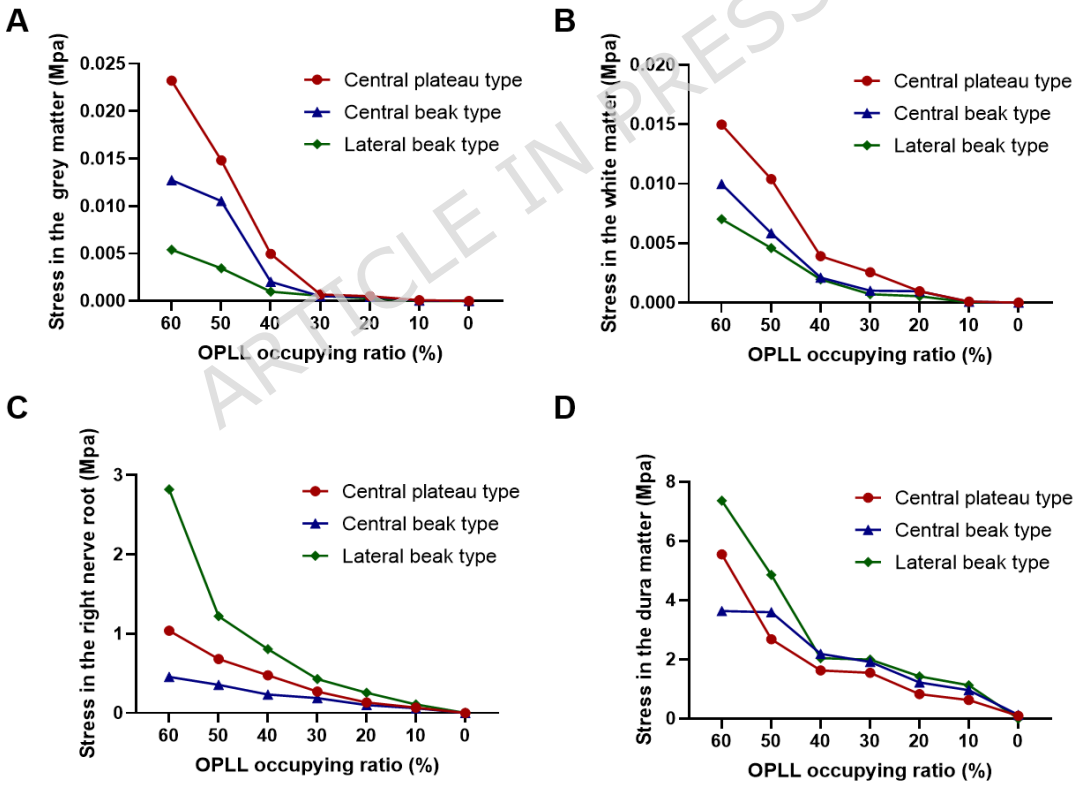

Fig. 5. Stress peaks in three groups of C-OPLL models: A: gray matter; B: white matter; C: nerve roots; D: dura mater.

4.Discussion

ACAF is a relatively novel anterior decompression technique for C-OPLL. Its surgical principle involves achieving spinal cord

decompression by anteriorly displacing the vertebral body-ossification complex en bloc via an anterior approach. The literature reports that its clinical effect is satisfactory [6,29]. However, there is a lack of quantitative data on the changes in spinal cord stress during this procedure. The pattern of spinal cord and nerve root stress changes during specific decompression operations has not been reported in relevant studies. And it is not known whether there are differences in spinal cord and nerve root stress changes and decompression effects between different types of C-OPLLs operated with this technique. This study represents the first finite element analysis to dynamically simulate and quantify the biomechanical evolution of spinal cord stress during the unique "controllable anterior displacement" mechanism of the ACAF procedure. In contrast to previous finite element studies focused on laminoplasty or ACCF/ACDF, our work systematically elucidates the distinctive decompression dynamics of ACAF and its interaction with different OPLL morphologies (central-plateau, central-beak, and lateral-beak types). We found that at a 60% encroachment ratio, the central-plateau type produced the highest stress on the gray and white matter. In contrast, the right-beak type of C-OPLL had the greatest stress on the nerve roots and dura mater, and the central-beak type of C-OPLL had the greatest stress on the gray matter, white matter, nerve roots, and dura mater in between. By simulating ACAF treatment of these three types of C-OPLL, it was found to have a better decompression effect on all three types of C-OPLL. As the proportion of vertebral body ossification encroaching on the spinal canal decreased during decompression, the stresses in the gray and white matter decreased most significantly in the central-plateau type of C-OPLL, followed by those in the central-beak type of C-OPLL. the lateral-beak type of C-OPLL exhibited the most significant decrease in stress within the nerve roots and dura mater. As the percentage of encroachment decreased further, the stress changes in gray matter, white matter, nerve root and dura mater converged among the types.

As the vertebral canal occupation of C-OPLL increases, the available space for the spinal cord decreases [30]. It has been reported that C-OPLL occupying more than 60% of the vertebral canal may be a risk factor for the development of spinal cord disease [31]. In our study, the central subtypes (plateau and beak) induced higher compressive stress on the spinal cord than the lateral (right-beak) subtype. This finding is consistent with the experimental results of Khuyagbaatar et al. [32] and is likely inextricably linked to the pathoanatomic relationship [30]. This is likely because the central-plateau subtype has a larger

cross-sectional area, occupying more spinal canal volume and thus exerting greater pressure on the spinal cord than the other subtypes. Whereas the C-OPLL of the right-beak type is located on one side, it is more likely to compress the nerve roots and surrounding dura mater involving its lateral saphenous foramen, leading to an increase in compressive stress in these areas. Based on our model, a residual encroachment ratio of approximately 30% or less may be biomechanically acceptable when complete anterior displacement is not achieved. This aligns with the critical value of encroachment ratio at which patients are considered for conservative versus surgical treatment [33,34]. Combined with previous discussions in clinical literature regarding spinal canal encroachment ratio and surgical indications, this mechanical inflection point may hold certain clinical reference significance. However, translating it directly into an 'acceptable' clinical threshold requires caution. The final clinical decision must comprehensively consider factors including the patient's symptoms, overall imaging presentation, and surgical risks. Furthermore, the applicability of this reference value may be limited in cases such as lateral beak-type OPLL, where the relief of nerve root stress may be delayed.

Due to the relatively recent development of the ACAF technique, biomechanical studies on it are scarce. At present, posterior single-door surgery is still the most classic surgical procedure for the treatment of C-OPLL, and through biomechanical methods, the effects of surgical methods on spinal cord stress have also been investigated in the literature [35,36], which can provide a more intuitive response to the decompression principle of the surgical procedure. Stoner et al. [36] compared spinal cord stress strains between anterior cervical discectomy and fusion with laminectomy and double-door laminoplasty by means of finite element modeling, and found that all procedures reduced the spinal cord stress strains at the operative site. Although ACAF is a distinct anterior approach, our study similarly demonstrated a gradual reduction in compressive stresses on the spinal cord, nerve roots, and dura mater at the surgical site during decompression. After simulating spinal cord compression with C-OPLL, Sim et al. concluded that a large focal C-OPLL would require a technique capable of creating sufficient and direct decompression space anterior to the spinal cord [37]. The decompression characteristics of ACAF are exactly what is needed when treating large focal C-OPLL. Nishida et al found that posterior decompression reduced the pressure in neutral spinal cord position, but the pressure on the spinal cord may increase with disc activity[38]. Therefore, the

fusion-fixation feature of ACAF may also be beneficial for the treatment of C-OPLL with kyphosis.

Regarding the reduction of nerve root and dural compression, ACAF effectively decompressed both structures across all three C-OPLL subtypes. However, the decompression pattern was unique for the right-beak type of C-OPLL. The nerve root decompression efficiency of the right-beak type C-OPLL plateaued at encroachment ratios of 60% to 50% and 40% to 30%. We hypothesize that this may occur because the ossified mass in the right-beak type is influenced by the anatomical constraints of the vertebral pedicle and lateral recess [32]. Its effective spinal canal diameter is small, and when compression reaches a certain level, the tensile load on the nerve roots enters a plateau range. When the compressed spinal cord is re-exacerbated or decompressed, the spinal cord appears to undergo large deformations that can again pull or release the nerve roots, resulting in large fluctuations in nerve-root stress. In addition, the dural decompression efficiency of the central-beak C-OPLL plateaued at encroachment ratios of 60% to 50% and 40% to 30%. This may be related to the area of compression and the compensatory space of the dura mater [39], which is smaller in the central-beak type than in the central-plateau type when compression is applied to the flatter dura mater in front. Therefore, small changes in the degree of compression may cause the stress values to plateau. However, as the ACAF continued to progressively decompress, the stress values of the nerve roots and dura mater gradually decreased in all three types of C-OPLL. In terms of clinical significance, this helps relieve nerve-root and dural symptoms [29]. Many anatomical and MRI studies have confirmed the existence of connections between the musculoskeletal system and the dura mater. Dural compression can lead to the release of mast cells and substance P, which are implicated in headaches and cervical discomfort [40,41]. For lateral beak-type OPLL, even when the overall encroachment ratio is reduced to 30%, the model still shows higher stress in the ipsilateral nerve root region. This suggests that if adhesions are present, achieving sufficient lateral decompression may require a larger degree of anterior displacement, thereby potentially increasing the risk of intraoperative dural traction or tear.

There are some limitations in this study. First, there may be some deviations in the establishment of the finite element model, leading to uncertainty in the results of the stress distribution analysis; second, this in silico (finite element) study fails to adequately consider the effects of individual patient differences, surgical operation techniques, and other factors on the surgical

results. In addition, referring to the previous study [35], spinal-cord material properties were based on bovine experimental data, and the subsequent studies on this aspect of human spinal cord properties should be supplemented. This study employed static analysis and did not incorporate flexion-extension, rotation, or inertial loads. Although ACAF fusion eliminates abnormal micromotion at the operated segments, it may transfer range of motion to adjacent levels, leading to dynamic redistribution of spinal cord stress. Future work should develop a dynamic finite-element model that includes viscoelastic ligaments, muscle-driven loading, and full cervical-spine six-degree-of-freedom kinematics to assess immediate postoperative and long-term spinal-cord safety boundaries under physiological motion. Furthermore, it must be explicitly emphasized that the "30% residual encroachment ratio" derived from this model is solely a biomechanical observation within the context of this study. The clinically acceptable threshold must be comprehensively evaluated by integrating the patient's neurological status and surgical risks. Finally, the model simplified the complexity of surgical procedures such as the anterior displacement of ossified masses posterior to the C4 and C5 vertebrae. Future finite element studies should incorporate material properties and connections to simulate adhesive tissues, as well as account for more ossified segments and types, to more accurately evaluate the biomechanical safety of the ACAF procedure under complex pathological conditions.

5.Conclusion

In summary, our biomechanical analysis demonstrates that the ACAF procedure produces effective decompression across all three C-OPLL subtypes (central-plateau, central-beak, and right-beak). The early decompression effect on white and gray matter was most significant in the central-plateau type, while nerve root and dural decompression was most pronounced in the right-beak type. Furthermore, the model data suggest that reducing the residual encroachment ratio to approximately 30% may represent a biomechanical inflection point, beyond which the marginal benefit of further decompression for the spinal cord plateaus. This biomechanical threshold necessitates careful clinical interpretation, integrating patient-specific neurological status and surgical risks.

Data availability

The datasets generated during and analysed during the current study are available from the corresponding author on reasonable request.

Author contributions

Xiao Zhang and Wenbo Gu contributed equally to this work.

Xiao Zhang, Wenbo Gu and Haifeng Yuan were responsible for the overall design of the study, processing of bioinformatics data, and writing of the manuscript. Donghui Cao, Xusheng Li, Hongyang Zhao, Yu Yang and Xi Zhu were responsible for data analysis and figure preparation. All authors read and approved the final manuscript.

Acknowledgements

We would like to thank the editors and reviewers of this journal for their work on this study.

Funding

This work was supported by the Ningxia Natural Science Foundation Project (grant 2023AAC03543).

Declarations

Competing interests

The authors declare no competing interests.

Ethics approval and consent to participate

The study protocol was reviewed and cleared by the Ethics Committee of the General Hospital of Ningxia Medical University (approval No. KYLL-2023-0583). The participant provided written consent and was free to withdraw at any time; the study protocol complied with the 2013 Declaration of Helsinki.

Consent for publication

All authors have read and approved the final submitted manuscript.

References

1. Boody BS, Lendner M, Vaccaro AR. Ossification of the posterior longitudinal ligament in the cervical spine: areview. Int Orthop. 2019;43(4):797-805. Epub 2019/4/1. doi: 10.1007/s00264-018-4106-5. PubMed 30116867.

2. Kawaguchi Y, Nakano M, Yasuda T, Seki S, Hori T, Kimura T. Ossification of the posterior longitudinal ligament in not only the cervicalspine, but also other spinal regions: analysis using multidetector computedtomography of the whole spine. Spine (Phila Pa 1976). 2013;38(23):E1477-82. Epub 2013/11/1. doi: 10.1097/BRS.0b013e3182a54f00. PubMed 23883833.

3. Yu H, Li X, Chen S, Zhang L, Yang G, Welle K, et al. Comparative Effectiveness and Safety of Anterior Cervical Corpectomy with Fusion,Laminoplasty, and Laminectomy and Instrumented Fusion for Ossification of thePosterior Longitudinal Ligament: A Systematic Review and Network Meta-Analysis. J Invest Surg. 2022;35(3):667-676. Epub 2022/3/1. doi: 10.1080/08941939.2020.1871535. PubMed 33472478.

4. Sun J, Shi J, Xu X, Yang Y, Wang Y, Kong Q, et al. Anterior controllable antidisplacement and fusion surgery for the treatment ofmultilevel severe

ossification of the posterior longitudinal ligament withmyelopathy: preliminary clinical results of a novel technique. Eur Spine J. 2018;27(6):1469-1478. Epub 2018/6/1. doi: 10.1007/s00586-017-5437-4. PubMed 29285560.

5. Sun K, Wang S, Sun J, Wang H, Huan L, Sun X, et al. Surgical Outcomes After Anterior Controllable Antedisplacement and FusionCompared with Single Open-Door Laminoplasty: Preliminary Analysis ofPostoperative Changes of Spinal Cord Displacements on T2-Weighted MagneticResonance Imaging. World Neurosurg. 2019;127:e288-e298. Epub 2019/7/1. doi: 10.1016/j.wneu.2019.03.108. PubMed 30902779.

6. Yang H, Xu X, Shi J, Guo Y, Sun J, Shi G, et al. Anterior Controllable Antedisplacement Fusion as a Choice for Ossification ofPosterior Longitudinal Ligament and Degenerative Kyphosis and Stenosis:Postoperative Morphology of Dura Mater and Probability Analysis of EpiduralHematoma Based on 63 Patients. World Neurosurg. 2019;121:e954-e961. Epub 2019/1/1. doi: 10.1016/j.wneu.2018.10.052. PubMed 30326317.

7. Miao J, Sun J, Shi J, Chen Y, Chen D. A Novel Anterior Revision Surgery for the Treatment of Cervical Ossification ofPosterior Longitudinal Ligament: Case Report and Review of the Literature. World Neurosurg. 2018;113:212-216. Epub 2018/5/1. doi: 10.1016/j.wneu.2018.02.076. PubMed 29476997.

8. Li S, Peng J, Xu R, Zheng R, Huang M, Xu Y, et al. Comparison of the surgeries for the ossification of the posterior longitudinalligament-related cervical spondylosis: A PRISMA-compliant network meta-analysisand literature review. Medicine (Baltimore). 2021;100(9):e24900. Epub 2021/3/5. doi: 10.1097/MD.0000000000024900. PubMed 33655951.

9. Mo ZJ, Zhao YB, Wang LZ, Sun Y, Zhang M, Fan YB. Biomechanical effects of cervical arthroplasty with U-shaped disc implant onsegmental range of motion and loading of surrounding soft tissue. Eur Spine J. 2014;23(3):613-21. Epub 2014/3/1. doi: 10.1007/s00586-013-3070-4. PubMed 24154828.

10. Kameyama T, Hashizume Y, Sobue G. Morphologic features of the normal human cadaveric spinal cord. Spine (Phila Pa 1976). 1996;21(11):1285-90. Epub 1996/6/1. doi: 10.1097/00007632-199606010-00001. PubMed 8725917.

11. Xue F, Deng H, Chen Z, Yang H, Li Y, Yuan S, et al. Effects of cervical rotatory manipulation on the cervical spinal cord complexwith ossification of the posterior longitudinal ligament in the vertebral canal:A finite element study. Front Bioeng Biotechnol. 2023;11:1095587. Epub 2023/1/20. doi: 10.3389/fbioe.2023.1095587. PubMed 36714008.

12. Matsunaga S, Nakamura K, Seichi A, Yokoyama T, Toh S, Ichimura S, et al. Radiographic predictors for the development of myelopathy in patients withossification of the posterior longitudinal ligament: a multicenter cohort study. Spine (Phila Pa 1976). 2008;33(24):2648-50. Epub 2008/11/15. doi: 10.1097/BRS.0b013e31817f988c. PubMed 19011547.

13. Y L, J L, F W, L W, Y S. Influence of K-line on intraoperative and hidden blood loss in patients with ossification of the posterior longitudinal ligament when undergoing unilateral open-door laminoplasty. J Orthop Surg Res. 2021;16(1):34. doi: 10.1186/s13018-020-02181-9. PubMed.

14. Boruah S, Subit DL, Paskoff GR, Shender BS, Crandall JR, Salzar RS. Influence of bone microstructure on the mechanical properties of skull corticalbone - A combined experimental and computational approach. J Mech Behav Biomed Mater. 2017;65:688-704. Epub 2017/1/1. doi: 10.1016/j.jmbbm.2016.09.041. PubMed 27743944.

15. Bevill G, Easley SK, Keaveny TM. Side-artifact errors in yield strength and elastic modulus for human trabecularbone and their dependence on bone volume fraction and anatomic site. J Biomech. 2007;40(15):3381-8. Epub 2007/1/20. doi: 10.1016/j.jbiomech.2007.05.008. PubMed 17659290.

16. Liu JF, Shim VPW, Lee PVS. Quasi-static Compressive and Tensile Tests on Cancellous Bone in Human Cervical Spine. In: Prorok BC, Barthelat F, Korach CS, Grande-Allen KJ, Lipke E, Lykofatitits G et al., ^editors; 2013; New York, NY. Springer New York. pp. 109-118.

17. Kato Y, Kanchiku T, Imajo Y, Kimura K, Ichihara K, Kawano S, et al. Biomechanical study of the effect of degree of static compression of the spinalcord in ossification of the posterior longitudinal ligament. J Neurosurg Spine. 2010;12(3):301-5. Epub 2010/3/1. doi: 10.3171/2009.9.SPINE09314. PubMed 20192631.

18. Salvador CAF, Maia EL, Costa FH, Escobar JD, Oliveira JP. A compilation of experimental data on the mechanical properties and microstructural features of Ti-alloys. Sci Data. 2022;9(1):188. PubMed Salvador2022.

19. Nikonovich M, Costa JFS, Fonseca AC, Ramalho A, Emami N. Structural, thermal, and mechanical characterisation of PEEK-based composites in cryogenic temperature. Polym Test. 2023;125:108139. doi: 10.1016/j.polymertesting.2023.108139. PubMed.

20. Hasler EM, Herzog W, Wu JZ, Müller W, Wyss U. Articular cartilage biomechanics: theoretical models, material properties, andbiosynthetic response. Crit Rev Biomed Eng. 1999;27(6):415-88. Epub 1999/1/19. PubMed 10952106.

21. Ichihara K, Taguchi T, Shimada Y, Sakuramoto I, Kawano S, Kawai S. Gray matter of the bovine cervical spinal cord is mechanically more rigid andfragile than the white matter. J Neurotrauma. 2001;18(3):361-7. Epub 2001/3/1. doi: 10.1089/08977150151071053. PubMed 11284555.

22. Persson C, Evans S, Marsh R, Summers JL, Hall RM. Poisson's ratio and strain rate dependency of the constitutive behavior of spinaldura mater. Ann Biomed Eng. 2010;38(3):975-83. Epub 2010/3/1. doi: 10.1007/s10439-010-9924-6. PubMed 20087767.

23. Nishida N, Kanchiku T, Ohgi J, Ichihara K, Chen X, Taguchi T. Mechanical properties of nerve roots and rami radiculares isolated from fresh

pigspinal cords. Neural Regen Res. 2015;10(11):1869-73. Epub 2015/11/1. doi: 10.4103/1673-5374.170319. PubMed 26807127.

24. Cheng S, Tan K, Bilston LE. The effects of the interthalamic adhesion position on cerebrospinal fluiddynamics in the cerebral ventricles. J Biomech. 2010;43(3):579-82. Epub 2010/2/10. doi: 10.1016/j.jbiomech.2009.10.002. PubMed 19896132.

25. Polak K, Czyż M, Ścigała K, Jarmundowicz W, Będziński R. Biomechanical characteristics of the porcine denticulate ligament in differentvertebral levels of the cervical spine-preliminary results of an experimentalstudy. J Mech Behav Biomed Mater. 2014;34:165-70. Epub 2014/6/1. doi: 10.1016/j.jmbbm.2014.02.010. PubMed 24583921.

26. Kong QJ, Sun XF, Wang Y, Sun PD, Sun JC, Ouyang J, et al. New anterior controllable antedisplacement and fusion surgery for cervicalossification of the posterior longitudinal ligament: a biomechanical study. J Neurosurg Spine. 2022:1-9. Epub 2022/1/7. doi: 10.3171/2021.8.SPINE21879. PubMed 34996038.

27. Hung TK, Lin HS, Bunegin L, Albin MS. Mechanical and neurological response of cat spinal cord under static loading. Surg Neurol. 1982;17(3):213-7. Epub 1982/3/1. doi: 10.1016/0090-3019(82)90284-1. PubMed 7079940.

28. Stoner KE, Abode-Iyamah KO, Magnotta VA, Howard MA, Grosland NM. Measurement of in vivo spinal cord displacement and strain fields of healthy andmyelopathic cervical spinal cord. J Neurosurg Spine. 2019;31(1):53-59. Epub 2019/3/22. doi: 10.3171/2018.12.SPINE18989. PubMed 30901756.

29. Luo X, Wang S, Sun K, Sun J, Wang Y, Jiang J, et al. Anterior Controllable Antedisplacement and Fusion (ACAF) Technique for theTreatment of Multilevel Cervical Spondylotic Myelopathy With Spinal Stenosis(MCSMSS): A Retrospective Study of 54 Cases. Clin Spine Surg. 2021;34(9):322-330. Epub 2021/11/1. doi: 10.1097/BSD.0000000000001144. PubMed 34379608.

30. SA R. Normal anatomy of the spinal cord. Pract Neurol. 2012;12(6):367-70. doi: 10.1136/practneurol-2012-000247. PubMed.

31. Lee J, Satkunendrarajah K, Fehlings MG. Development and characterization of a novel rat model of cervical spondyloticmyelopathy: the impact of chronic cord compression on clinical, neuroanatomical,and neurophysiological outcomes. J Neurotrauma. 2012;29(5):1012-27. Epub 2012/3/20. doi: 10.1089/neu.2010.1709. PubMed 21561323.

32. Khuyagbaatar B, Kim K, Park WM, Kim YH. Influence of sagittal and axial types of ossification of posterior longitudinalligament on mechanical stress in cervical spinal cord: A finite element analysis. Clin Biomech (Bristol, Avon). 2015;30(10):1133-9. Epub 2015/12/1. doi: 10.1016/j.clinbiomech.2015.08.013. PubMed 26351002.

33. He Q, Lv Z, Hu Y, Chen C, Zhan E, Wang X, et al. Comparison of anterior vs. posterior surgery for cervical myelopathy due to OPLL:a systematic review and meta-analysis. Ann Med Surg (Lond).

2024;86(11):6653-6664. Epub 2024/11/1. doi: 10.1097/MS9.0000000000002556. PubMed 39525719.

34. Sun N, Jiang C, Liu Y. Surgical options for ossification of the posterior longitudinal ligament of thecervical spine: a narrative review. J Orthop Surg Res. 2024;19(1):707. Epub 2024/11/1. doi: 10.1186/s13018-024-05215-8. PubMed 39487441.

35. Khuyagbaatar B, Kim K, Purevsuren T, Lee SH, Kim YH. Biomechanical Effects on Cervical Spinal Cord and Nerve Root FollowingLaminoplasty for Ossification of the Posterior Longitudinal Ligament in theCervical Spine: A Comparison Between Open-Door and Double-Door Laminoplasty UsingFinite Element Analysis. J Biomech Eng. 2018;140(7)Epub 2018/7/1. doi: 10.1115/1.4039826. PubMed 29677281.

36. Stoner KE, Abode-Iyamah KO, Fredericks DC, Viljoen S, Howard MA, Grosland NM. A comprehensive finite element model of surgical treatment for cervicalmyelopathy. Clin Biomech (Bristol, Avon). 2020;74:79-86. Epub 2020/4/1. doi: 10.1016/j.clinbiomech.2020.02.009. PubMed 32145673.

37. Sim O, Ryu D, Lee J, Lee C. Stress Distribution on Spinal Cord According to Type of Laminectomy for LargeFocal Cervical Ossification of Posterior Longitudinal Ligament Based on FiniteElement Method. Bioengineering (Basel). 2022;9(10)Epub 2022/10/2. doi: 10.3390/bioengineering9100519. PubMed 36290487.

38. Nishida N, Jiang F, Asano T, Tome R, Kumaran Y, Imajo Y, et al. Effect of posterior decompression with and without fixation on a kyphoticcervical spine with ossification of the posterior longitudinal ligament. Spinal Cord. 2023;61(2):133-138. Epub 2023/2/1. doi: 10.1038/s41393-022-00857-z. PubMed 36216915.

39. M P, JP P, SH K, YJ C. Evaluation of dural channels in the human parasagittal dural space and dura mater. Annals of anatomy = Anatomischer Anzeiger : official organ of the Anatomische Gesellschaft. 2022;244:151974. doi: 10.1016/j.aanat.2022.151974. PubMed.

40. Palomeque-Del-Cerro L, Arráez-Aybar LA, Rodríguez-Blanco C, Guzmán-García R, Menendez-Aparicio M, Oliva-Pascual-Vaca Á. A Systematic Review of the Soft-Tissue Connections Between Neck Muscles and DuraMater: The Myodural Bridge. Spine (Phila Pa 1976). 2017;42(1):49-54. Epub 2017/1/1. doi: 10.1097/BRS.0000000000001655. PubMed 27116115.

41. Panzer MB, Myers BS, Capehart BP, Bass CR. Development of a finite element model for blast brain injury and the effects ofCSF cavitation. Ann Biomed Eng. 2012;40(7):1530-44. Epub 2012/7/1. doi: 10.1007/s10439-012-0519-2. PubMed 22298329.